Critical behavior of the quantum contact process in one dimension

Federico Carollo,[1,2] Edward Gillman,[1,2] Hendrik Weimer,[3] and Igor Lesanovsky[1,2]

[1] *School of Physics and Astronomy, University of Nottingham, Nottingham, NG7 2RD, UK*
[2] *Centre for the Mathematics and Theoretical Physics of Quantum Non-Equilibrium Systems, University of Nottingham, Nottingham, NG7 2RD, UK*
[3] *Institut für Theoretische Physik, Leibniz Universität Hannover, Appelstraße 2, 30167 Hannover, Germany*

(Dated: August 14, 2019)

The contact process is a paradigmatic classical stochastic system displaying critical behavior even in one dimension. It features a non-equilibrium phase transition into an absorbing state that has been widely investigated and shown to belong to the directed percolation universality class. When the same process is considered in a quantum setting much less is known. So far mainly semi-classical studies have been conducted and the nature of the transition in low dimensions is still a matter of debate. Also from a numerical point of view, from which the system may look fairly simple — especially in one dimension — results are lacking. In particular the presence of the absorbing state poses a substantial challenge which appears to affect the reliability of algorithms targeting directly the steady-state. Here we perform real-time numerical simulations of the open dynamics of the quantum contact process and shed light on the existence and on the nature of an absorbing state phase transition in one dimension. We find evidence for the transition being continuous and provide first estimates for the critical exponents. Beyond the conceptual interest, the simplicity of the quantum contact process makes it an ideal benchmark problem for scrutinizing numerical methods for open quantum non-equilibrium systems.

Introduction – Understanding the non-equilibrium behavior of many-body quantum systems is one of the major goals of current research in physics. From the experimental side, recent technological developments and increased capabilities in the realisation and control of quantum systems offer promising platforms for the investigation of quantum phenomena far from equilibrium [1–12]. However, from a theoretical perspective, non-equilibrium quantum systems are typically much more complex than classical ones and their characterization is still an open problem, especially when going beyond the realm of exactly solvable models or the application of semi-classical approaches [13–20]. Even numerical studies, which in the classical case allow for the accurate investigation of non-integrable systems, in quantum settings are often severely limited due to computational constraints.

A paradigmatic example — illustrating the gap in our understanding of classical and quantum non-equilibrium systems — is the *contact process*. A contact process model deals with a d-dimensional lattice system, whose sites can be either empty or occupied by a particle. In a classical setting, the dynamics is given by two incoherent processes: (i) *self-destruction*, consisting of spontaneous particle decay, and (ii) *branching* (*coagulation*) for which an empty (occupied) site can become occupied (empty) only if at least one particle is present in the neighboring sites [*cf.* Fig. 1(a)]. The non-equilibrium behavior resulting from these dynamical rules has been widely investigated, as it is relevant for e.g. epidemic spreading or growth of bacterial colonies [21–23], and these systems exhibit second-order absorbing state phase transitions, which belong to the *directed percolation* (DP) universality class [24–26].

An interesting situation emerges when *branching/coagulation* is promoted from a probabilistic to a coherent process, see Fig. 1(b). Little is known in this quantum regime. Understanding such minimal model of a quantum non-equilibrium dynamics is thus certainly of substantial academic interest. A further aspect making this model so appealing is that it can be realised on recently developed quantum simulators based on Rydberg atoms [27–29]. Using mean-field theory approximations, i.e. neglecting correlations among sites, it was found that the absorbing state phase transition of the contact process survives in the quantum regime [30–32]. However, these results also suggest that the transition is of first-order for any lattice dimension. This contradicts the common belief that discontinuous transitions

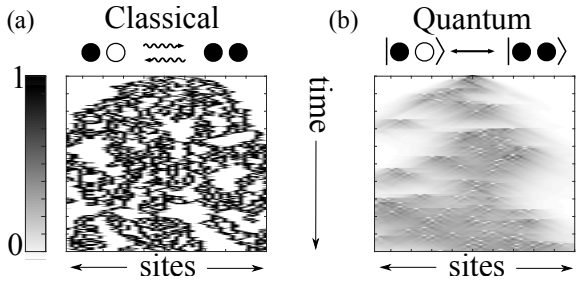

FIG. 1. **Classical vs. quantum dynamics.** (a) Trajectory with incoherent branching (coagulation) process: an empty (occupied) site can become occupied (empty) if at least one of the neighboring sites is occupied. Within a given trajectory sites are either empty or occupied. (b) Trajectory of the quantum process, where branching (coagulation) is driven coherently by a Hamiltonian. Superposition of different configurations are generated within a single trajectory and the density hence assumes values that are in between zero and one.

should not occur in generic non-equilibrium $1d$ systems with fluctuating ordered phases [33] and a softening of the transition into a second-order one has been conjectured [34]. This clearly shows that efforts to capture the physics of the quantum contact process must go beyond semi-classical approaches and use techniques which leave quantum correlations between different sites intact.

In this paper, we conduct a detailed investigation of the $1d$ quantum contact process (QCP) and make substantial steps towards a comprehensive understanding of the critical behavior of this challenging quantum non-equilibrium problem. Applying the *infinite time-evolving block decimation* (iTEBD) algorithm, we find evidence for a continuous non-equilibrium phase transition. We also establish an estimate for the location of the critical point and provide estimates for the critical exponents, which suggest that the universality class is in fact different from that of (classical) directed percolation.

The model - To model the QCP for a finite size system, we consider a chain of L sites with open boundaries. Attached to each site there is a two-level system with basis $\{|\bullet\rangle, |\circ\rangle\}$, representing occupied and empty sites respectively. The evolution of the quantum state $\rho(t)$ is governed by Lindblad generators [35–38], $\dot{\rho}(t) = \mathcal{L}[\rho(t)]$, with $\mathcal{L}[\rho] = -i[H, \rho] + \mathcal{D}[\rho]$. The purely dissipative contribution to the dynamics, $\mathcal{D}[\rho]$, encodes the (classical) spontaneous particle decay ($|\bullet\rangle \to |\circ\rangle$):

$$\mathcal{D}[\rho] = \gamma \sum_{k=1}^{L} \left(\sigma_-^{(k)} \rho \sigma_+^{(k)} - \frac{1}{2} \left\{ n^{(k)}, \rho \right\} \right) , \qquad (1)$$

where $\sigma_-|\bullet\rangle = |\circ\rangle$, $\sigma_-|\circ\rangle = 0$, and $\sigma_+ = \sigma_-^\dagger$ are the ladder spin operators, while $n = \sigma_+\sigma_-$ is the number operator. The Hamiltonian H, instead, encodes the coherent version of the branching/coagulation process and has the form [30, 31, 34] (with $\sigma_1|\bullet/\circ\rangle = |\circ/\bullet\rangle$),

$$H = \Omega \sum_{k=1}^{L-1} \left(\sigma_1^{(k)} n^{(k+1)} + n^{(k)} \sigma_1^{(k+1)} \right) . \qquad (2)$$

The structure of this Hamiltonian is such that the state of a site can (coherently) evolve only if at least one of the neighboring sites is occupied.

By construction, the vacuum state $\rho_0 = |0\rangle\langle 0|$, with $|0\rangle = \bigotimes_{k=1}^{L} |\circ\rangle$, is a steady-state of the open system dynamics. This is an absorbing state, characterized by zero dynamical fluctuations. In the classical contact process, an additional steady-state can emerge in the thermodynamic limit and for sufficiently large values of the branching rate. This state has a finite density of particles, and at a critical branching rate one observes a non-equilibrium absorbing state phase transition, which belongs to the DP universality class [24–26].

Numerical methods - The numerical simulation of quantum dissipative dynamics remains a major challenge [39–46]. Exact diagonalization of the Lindblad generator is limited to small systems for which the transition in the QCP cannot be detected. To study larger systems [47, 48], one needs to resort to approximate representations of the quantum state, e.g. through *matrix product states* (MPSs) [49, 50]. A possible way to study a non-equilibrium phase transition is thus offered by MPS techniques targeting the steady-state of the dynamics [51, 52]. However, in the case of non-equilibrium phase transitions, universal information is also contained in the dynamics itself. Furthmore, for our model, we observe that these methods struggle to pinpoint the transition, as they tend to be biased towards the uncorrelated (absorbing) steady-state, ρ_0, in any parameter regime. For these reasons, we run real-time dynamical simulations by means of TEBD algorithms [53–56], working in the thermodynamic limit (iTEBD). These simulations directly implement the open system dynamics in Liouville space [57, 58]. Their accuracy is limited by a finite bond dimension χ in the approximation of the evolved state. Nonetheless, this strategy currently seems to be the only one possible, among existing algorithms, to study the QCP. For our simulations we used different Trotter schemes with time-steps (time is given in units of γ^{-1}, throughout), $0.01 \leq dt \leq 0.1$, and $\chi \leq 1300$, reaching simulation times $t \approx 50$ on standard PCs.

Non-equilibrium phase transition - As a first step, we establish the existence of an absorbing state phase transition in the QCP and estimate the location of the critical point, Ω_c. The order parameter is the average number of particles, $n(t) = L^{-1} \sum_k \mathrm{Tr}\left(\rho(t) n^{(k)}\right)$, which is zero in the absorbing phase, $\Omega < \Omega_c$, and non-zero in the finite-density phase $\Omega > \Omega_c$.

To establish these phases numerically we estimate the quasi-stationary density, n_{qs}, by using the approximation of $n(t)$ obtained from the iTEBD simulations, for sufficiently large values of t where the density is approximately stationary, see Fig. 2(a). With a bond dimension of $\chi \leq 800$ we can establish convergence of $n(t)$ up to $\Omega \approx 3$ [see Fig. 2(b)]. For these values, we find that the density $n(t)$ decays exponentially to zero and $n_{\mathrm{qs}} \approx 0$. Thus, this region belongs to the absorbing phase. For larger Ω it becomes challenging to establish convergence (see discussion further below). However, when $\Omega \geq 8$ it again becomes possible to approximate n_{qs} with $\chi \leq 800$. The density n_{qs} is found to be non-zero, which establishes the existence of an active phase and pins down the phase transition region to the interval $3 < \Omega_c < 8$. Here long relaxation times together with the concomitant buildup of entanglement and quantum correlations require a large MPS bond dimension for establishing convergence. This is visible in the stationary density displayed in Fig. 2(b), whose shape is suggestive of a second-order phase transition, smoothed by finite time effects.

The different phases of the QCP become also visible in single dynamical realizations starting from a single seed,

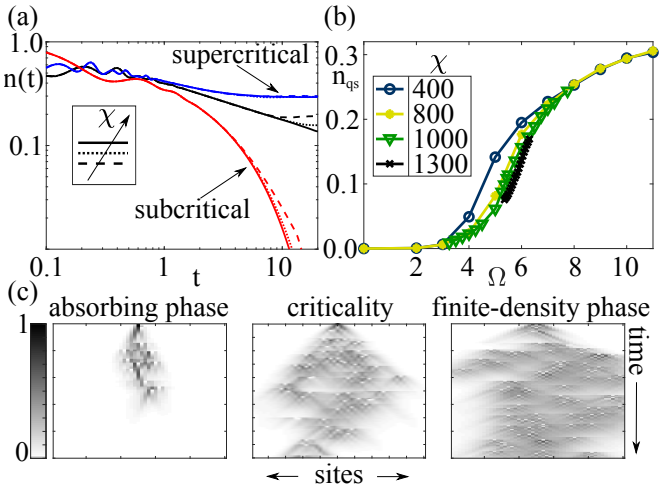

FIG. 2. **Infinite-system simulations.** (a) Log-log plot of the density $n(t)$. For $\Omega = 2$ (bottom curves with $\chi = 50, 100, 200$), a rapid convergence to an exponentially decaying curve is observed. For $\Omega = 10$ (top curves with $\chi = 200, 400, 800$) instead a convergence to a stationary finite density curve is shown. Curves in the middle are for $\Omega = 6$: here, larger bond dimensions ($\chi = 350, 1000, 1300$) are needed because of entanglement and correlation growth in the MPS close to criticality. (b) Quasi-stationary density $n_{\rm qs}$ (taken at $t = 20$): its dependence on Ω seems to suggest a continuous transition. (c) **Finite-system simulations**. $L = 50$ and $\chi = 300$. Density-plot of the site-resolved average density for representative quantum trajectories starting from a single seed. The initial state is the one with a single occupied site. Times and rates are in units of γ^{-1} and γ, respectively.

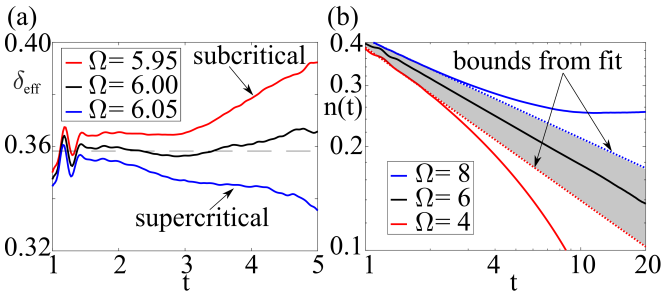

FIG. 3. **Determination of δ-exponent from infinite-system simulations.** (a) Plot of the effective exponent $\delta_{\rm eff}(t)$ of Eq. (4), with $b = 4$. For $\Omega = 5.95$ the exponent increases at later times signaling that the curve is subcritical; this provides a lower bound for Ω_c. On the contrary, $\Omega = 6.05$ looks supercritical. For $\Omega = 6$ we observe an almost constant behavior; we thus consider $\Omega_c \approx 6$. The dashed line guides the eye to the value $\delta = 0.358$, obtained by averaging the latter curve for $t \in [1.5, 3]$. (b) An uncertainty range for δ is obtained by extrapolating an algebraic behavior from two converged (in χ) curves bounding Ω_c. The fit is performed for $t \in [1, 2]$, providing $\delta \in [0.28, 0.44]$. Times and rates are in units of γ^{-1} and γ, respectively.

displayed in Fig. 2(c). In the absorbing phase the seed creates a small cluster which does not spread and rapidly dies. In the active phase, instead, the branching process is dominant and the initial seed spreads populating the whole system. In the critical region, a contained propagation can be observed, and the density still tends to zero for later times.

Critical behavior and exponents: universal dynamics - We start the analysis of the critical region by studying dynamical observables. The location of the critical point Ω_c can be established by analyzing the time evolution of $n(t)$, as shown in Fig. 2(a): the concavity of this curve, in a log-log plot, can indicate whether the corresponding Ω is supercritical (positive concavity) or subcritical (negative concavity). This allows us to improve the estimate for Ω_c, particularly when combined with the observation that the finite bond-dimension effects consistently lead to an artificial saturation of $n(t)$ at a finite value [*cf.* Fig. 2(a)-(b)]. Therefore, once a value of Ω is established to be in the absorbing phase for some χ, we can be confident that it is also so as $\chi \to \infty$. This makes it possible establish a lower-bound on Ω_c by simply taking the highest χ simulations available and checking which $n(t)$-curves lie in the inactive phase. Of course, this also means that establishing an upper bound is more challenging and from analyzing our data we conclude that Ω_c must be in the range $\Omega_c \in [5.95, 7]$.

Under the assumption of a second-order absorbing state phase transition, the order parameter is expected to follow the universal scaling relation [26]

$$n(t) \approx t^{-\delta} f\left((\Omega - \Omega_c)\, t^{1/\nu_\parallel}\right) , \qquad (3)$$

where δ and $\nu_\parallel$ are critical exponents and f a universal scaling function. The exponent $\nu_\parallel$ is related to the divergence of the time-correlations, while δ determines the critical algebraic decay of the density, $n(t) \approx t^{-\delta} f(0)$, for $\Omega = \Omega_c$. To obtain an estimate for the critical point Ω_c we search for the $n(t)$-curve showing algebraic decay [see critical regime in Fig. 2(a)]. This is done by defining an effective exponent [26],

$$\delta_{\rm eff}(t) = -\frac{1}{\log b} \log \frac{n(t\, b)}{n(t)} , \qquad (4)$$

and identifying the Ω-value for which $\delta_{\rm eff}(t)$ is as close as possible to a constant. In this way, as is shown in Fig. 3(a), we can recover our best estimate both for the critical rate $\Omega_c \approx 6$ and for the exponent $\delta \approx 0.36$. To provide bounds on the latter value, we extrapolate an algebraic behavior from a converged (in bond dimension) subcritical curve and a supercritical one: taking $\Omega = 4$ to be the subcritical and $\Omega = 8$ to be the supercritical one, as shown in Fig. 3(b), we obtain $\delta = 0.36 \pm 0.08$.

The dynamical scaling relation (3) also implies that plotting $n(t)\, t^{\delta}$ as a function of $t\, |\Omega - \Omega_c|^{\nu_\parallel}$ should yield a collapse of all curves into two master curves, depending on whether the value of Ω is above or below critical.

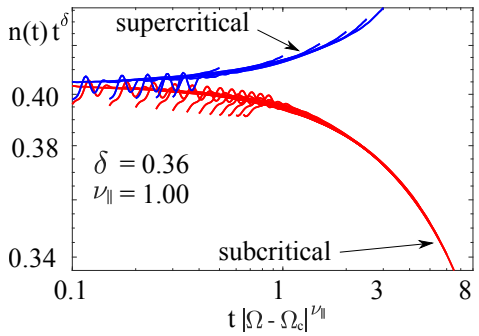

FIG. 4. **Determination of $\nu_\parallel$-exponent from infinite-system simulations.** Scaled average density, $n(t)\,t^\delta$, as a function of $t\,|\Omega-\Omega_c|^{\nu_\parallel}$ for $\chi = 1300$. The critical values $\delta = 0.36$, $\nu_\parallel = 1$ and $\Omega_c = 6$ collapse all curves into two master curves. The detachment of the supercritical curves for long times from the master one is likely a finite bond dimension effect: low bond dimensions appear to cause an artificial density saturation. Times and rates are in units of γ^{-1} and γ, respectively.

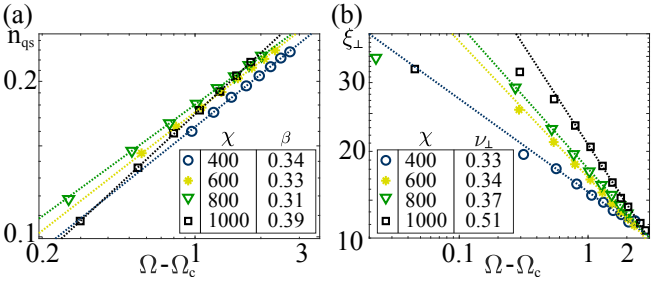

FIG. 5. **Steady-state exponents (β, $\nu_\perp$) from infinite-system simulations.** Plots in log-log scale with Ω in units of γ. (a) Extrapolation of β from the quasi-stationary density (taken at $t = 40$). Dashed lines are fits with power-law curves in the range $\Omega \in [5.5, 7]$. We can estimate $\beta = 0.39 \pm 0.08$: the value is obtained from the simulations with largest χ, while the error is the maximal distance of this from lower bond dimensions. (b) Correlation length $\xi_\perp$: the behavior is consistent with second-order phase transition as correlations increase in the critical region. Fits are obtained by discarding the data showing a rounding off of the correlations length due to finite χ effects.

Fig. 4 indeed shows such a collapse. This allows us to estimate $\nu_\parallel \approx 1$, and is a further hint towards the continuous nature of the phase transition.

Critical behavior and exponents: steady-state universality **-** Estimates for static critical exponents are obtained by analyzing the density $n_{\rm qs}$ [Fig. 2(b)] and the spatial correlation length $\xi_\perp$ near the critical point. These quantities are expected to behave as $n_{\rm qs} \approx |\Omega-\Omega_c|^\beta$ and $\xi_\perp \approx |\Omega-\Omega_c|^{-\nu_\perp}$, respectively, defining the critical exponents β and $\nu_\perp$.

The determination of static exponents is more challenging than that of the dynamical ones, as it requires a large number of simulations up to long times. Additionally, while the exponent δ can be bound easily from a single active and inactive realization of $n(t)$ [Fig. 3(b)], the values of β and $\nu_\perp$ are extracted from fits that are highly sensitive to the considered region of Ω-values. The determination of $\nu_\perp$ is particularly demanding as the correlation length constitutes a non-local observable, which is computed from the asymptotic behavior of the density-density correlation function, $C(r) = \langle n^{(r)} n^{(0)}\rangle - \langle n^{(0)}\rangle^2 \sim e^{-r/\xi_\perp}$. In the vicinity of critical points in second-order phase transition where long-range correlations are expected, such non-local observables are difficult to approximate, since MPSs only support a maximal correlation length set by the bond dimension.

To determine β we investigate the range $\Omega \approx [5, 7]$, performing a power-law fit with β and Ω_c treated as free parameters, see Fig. 5(a). As χ is increased, the estimate of Ω_c is shifted to higher values, which is consistent with the artificial saturation of the density due to a finite bond dimension. Our estimate for the exponent is $\beta = 0.39 \pm 0.08$, with error given by the largest distance of the estimate from lower bond-dimension results. This is compatible with the value of β obtained assuming the validity of a standard scaling relation for absorbing-state phase transitions [26]: $\beta = \delta\nu_\parallel \approx 0.36$.

Fig. 5(b) displays the behavior of the correlation length $\xi_\perp$ as estimated from the density-density correlation function. All data are consistent with a power-law behavior. Near the critical point the correlation length systematically increases with increasing bond dimension. This suggests that, for a large enough χ, one should be able to observe, close to criticality, diverging correlation lengths as expected in continuous transitions. However, our data are strongly affected by finite bond dimensions: near the critical point the correlation length rounds off instead of diverging. This is due to the fact that a finite bond dimension enforces a finite correlation length. This in turn means that we cannot provide a precise estimate of the exponent $\nu_\perp$. As a reference value, we can fit our results as done for obtaining β — in this case neglecting the points showing a rounding of the divergence — which yields $\nu_\perp = 0.5 \pm 0.2$ [59].

Summary and conclusions **-** We have found strong evidence of a continuous absorbing-state phase transition in the $1d$ QCP. Estimates for the critical exponents are summarized in Table I. As we exploited iTEBD algorithms, our results are free of finite-size effects. The main limitation arises from finite simulation times. Nevertheless, the simulation times are sufficiently large to observe signatures of critical scaling, which in particular in the case of the exponent δ is not compatible with the DP universality class in $1d$. This finding is further corroborated by finite size simulations provided in the supplemental material [59].

All exponents are, instead, remarkably close to those predicted for the tri-critical point of a mixed quantum

	QCP	$1d$ DP [26]	$2d$ DP [26]	$2d$ Ref. [31]
δ	0.36±0.08	0.16	0.45	0.35
β	0.39±0.08	0.28	0.58	0.35
$\nu_\perp$	0.5±0.2	1.10	0.73	0.52
$\nu_\parallel$	1*	1.73	1.30	1.03

TABLE I. Exponents of the QCP, as well as of the $1d$ and $2d$ DP [26]. The last column displays exponents for the tri-critical point of a quantum plus classical branching $2d$ process [31]. *Exponent estimated from data collapse in Fig. 4.

and classical contact process in $2d$ [31]. This might be a coincidence or could be rationalized as follows: Ref. [31] predicts a tri-critical point for quantum and classical branching, while a first-order transition for only quantum branching. As there appears to be no first-order transition in $1d$ this could mean that quantum fluctuations (to a large extent neglected in [31]) shift the tri-critical point onto the quantum axis –its occurrence does not require classical branching. However, the mismatch in the dimension, i.e. $1d$ vs $2d$, remains puzzling: this could indicate that a classical field-theoretical description of the $1d$ QCP requires an effective dimension $d = 2$, as suggested by preliminary comparisons of iTEBD results with finite-size classical scaling theory [59].

Acknowledgements **-** We thank Maryam Roghani, Matteo Marcuzzi, Jonathan Keeling and Mari-Carmen Banuls for fruitful discussions. We are grateful for access to the University of Nottingham's Augusta HPC service. The research leading to these results has received funding from the European Research Council under the European Unions Seventh Framework Programme (FP/2007-2013)/ERC [grant agreement number 335266 (ESCQUMA)], the Engineering and Physical Sciences Council [grant numbers EP/M014266/1, EP/N03404X/1 and EP/R04340X/1], the Leverhulme Trust [grant number RPG-2018-181], the Volkswagen Foundation and the DFG within EXC 2123 (QuantumFrontiers), SFB 1227 (DQ-mat), and SPP 1929 (GiRyd). IL gratefully acknowledges funding through the Royal Society Wolfson Research Merit Award.

[1] N. Syassen, D. M. Bauer, M. Lettner, T. Volz, D. Dietze, J. J. García-Ripoll, J. I. Cirac, G. Rempe, and S. Dürr, Science **320**, 1329 (2008).
[2] K. Kim, M. S. Chang, S. Korenblit, R. Islam, E. E. Edwards, J. K. Freericks, G. D. Lin, L. M. Duan, and C. Monroe, Nature **465**, 590 (2010).
[3] J. T. Barreiro, M. Müller, P. Schindler, D. Nigg, T. Monz, M. Chwalla, M. Hennrich, C. F. Roos, P. Zoller, and R. Blatt, Nature **470**, 486 (2011).
[4] M. Müller, S. Diehl, G. Pupillo, and P. Zoller, in *Advances in Atomic, Molecular, and Optical Physics*, Vol. 61, edited by P. Berman, E. Arimondo, and C. Lin (Academic Press, 2012) pp. 1 – 80.
[5] M. Schreiber, S. S. Hodgman, P. Bordia, H. P. Lüschen, M. H. Fischer, R. Vosk, E. Altman, U. Schneider, and I. Bloch, Science **349**, 842 (2015).
[6] J. Eisert, M. Friesdorf, and C. Gogolin, Nature Physics **11**, 124 (2015).
[7] R. Islam, R. Ma, P. M. Preiss, M. Eric Tai, A. Lukin, M. Rispoli, and M. Greiner, Nature **528**, 77 (2015).
[8] J. G. Bohnet, B. C. Sawyer, J. W. Britton, M. L. Wall, A. M. Rey, M. Foss-Feig, and J. J. Bollinger, Science **352**, 1297 (2016).
[9] H. P. Lüschen, P. Bordia, S. S. Hodgman, M. Schreiber, S. Sarkar, A. J. Daley, M. H. Fischer, E. Altman, I. Bloch, and U. Schneider, Phys. Rev. X **7**, 011034 (2017).
[10] V. Lienhard, S. de Léséleuc, D. Barredo, T. Lahaye, A. Browaeys, M. Schuler, L.-P. Henry, and A. M. Läuchli, Phys. Rev. X **8**, 021070 (2018).
[11] M. Lebrat, P. Grišins, D. Husmann, S. Häusler, L. Corman, T. Giamarchi, J.-P. Brantut, and T. Esslinger, Phys. Rev. X **8**, 011053 (2018).
[12] C. G. Wade, M. Marcuzzi, E. Levi, J. M. Kondo, I. Lesanovsky, C. S. Adams, and K. J. Weatherill, Nat. Commun. **9**, 3567 (2018).
[13] T. Prosen, New Journal of Physics **10**, 043026 (2008).
[14] T. Prosen and I. Pižorn, Phys. Rev. Lett. **101**, 105701 (2008).
[15] M. Žnidarič, J. Phys. A **43**, 415004 (2010).
[16] S. R. Clark, J. Prior, M. J. Hartmann, D. Jaksch, and M. B. Plenio, New Journal of Physics **12**, 025005 (2010).
[17] T. Prosen and E. Ilievski, Phys. Rev. Lett. **107**, 060403 (2011).
[18] T. Prosen, Phys. Rev. Lett. **107**, 137201 (2011).
[19] D. Karevski, V. Popkov, and G. M. Schütz, Phys. Rev. Lett. **110**, 047201 (2013).
[20] E. Ilievski, SciPost Phys. **3**, 031 (2017).
[21] D. Mollison, J. Roy. Stat. Soc. **B 39**, 283 (1977).
[22] P. Grassberger, Math. Biosci. **63**, 157 (1983).
[23] J.-T. Kuhr, M. Leisner, and E. Frey, New J. Phys. **13**, 113013 (2011).
[24] R. Dickman and I. Jensen, Phys. Rev. Lett. **67**, 2391 (1991).
[25] I. Jensen and R. Dickman, J. Stat. Phys. **71**, 89 (1993).
[26] H. Hinrichsen, Advances in Physics **49**, 815 (2000).
[27] R. Gutiérrez, C. Simonelli, M. Archimi, F. Castellucci, E. Arimondo, D. Ciampini, M. Marcuzzi, I. Lesanovsky, and O. Morsch, Phys. Rev. A **96**, 041602 (2017).
[28] S. Helmrich, A. Arias, and S. Whitlock, Phys. Rev. A **98**, 022109 (2018).
[29] S. Helmrich, A. Arias, G. Loachead, M. Buchhold, S. Diehl, and S. Whitlock, arXiv:1806.09931 (2018).
[30] M. Marcuzzi, M. Buchhold, S. Diehl, and I. Lesanovsky, Phys. Rev. Lett. **116**, 245701 (2016).
[31] M. Buchhold, B. Everest, M. Marcuzzi, I. Lesanovsky, and S. Diehl, Phys. Rev. B **95**, 014308 (2017).
[32] M. Jo, J. Um, and B. Kahng, arXiv:1901.07682 (2019).
[33] H. Hinrichsen, arXiv:0006212 (2000).
[34] D. Roscher, S. Diehl, and M. Buchhold, Phys. Rev. A **98**, 062117 (2018).
[35] V. Gorini, A. Kossakowski, and E. C. G. Sudarshan, J. Mat. Phys. **17**, 821 (1976).
[36] G. Lindblad, Comm. Math. Phys **48**, 119 (1976).
[37] H. P. Breuer and F. Petruccione, *The theory of open quantum systems* (Oxford University Press, Great Clarendon Street, 2002).
[38] C. Gardiner and P. Zoller, *Quantum noise* (Springer,

2004).
[39] L. Bonnes and A. M. Läuchli, arXiv:1411.4831 (2014).
[40] H. Weimer, Phys. Rev. Lett. **114**, 040402 (2015).
[41] F. A. Y. N. Schröder and A. W. Chin, Phys. Rev. B **93**, 075105 (2016).
[42] J. Jin, A. Biella, O. Viyuela, L. Mazza, J. Keeling, R. Fazio, and D. Rossini, Phys. Rev. X **6**, 031011 (2016).
[43] A. H. Werner, D. Jaschke, P. Silvi, M. Kliesch, T. Calarco, J. Eisert, and S. Montangero, Phys. Rev. Lett. **116**, 237201 (2016).
[44] H.-B. Chen, C. Gneiting, P.-Y. Lo, Y.-N. Chen, and F. Nori, Phys. Rev. Lett. **120**, 030403 (2018).
[45] D. Jaschke, S. Montangero, and L. D. Carr, Quantum Science and Technology **4**, 013001 (2019).
[46] M. Raghunandan, J. Wrachtrup, and H. Weimer, Phys. Rev. Lett. **120**, 150501 (2018).
[47] T. Prosen and M. Žnidarič, J. Stat. Mech. **2009**, P02035 (2009).
[48] M. Ljubotina, M. Žnidarič, and T. Prosen, Nat. Commun. **8**, 16117 (2017).
[49] U. Schollwöck, Annals of Physics **326**, 96 (2011).
[50] S. Paeckel, T. Köhler, A. Swoboda, S. R. Manmana, U. Schollwöck, and C. Hubig, arXiv:1901.05824 (2019).
[51] J. Cui, J. I. Cirac, and M. C. Bañuls, Phys. Rev. Lett. **114**, 220601 (2015).
[52] A. A. Gangat, T. I, and Y.-J. Kao, Phys. Rev. Lett. **119**, 010501 (2017).
[53] G. Vidal, Phys. Rev. Lett. **93**, 040502 (2004).
[54] M. Zwolak and G. Vidal, Phys. Rev. Lett. **93**, 207205 (2004).
[55] G. Vidal, Phys. Rev. Lett. **98**, 070201 (2007).
[56] R. N. Pfeifer, G. Evenbly, S. Singh, and G. Vidal, arXiv:0006212 (2014).
[57] R. Orús and G. Vidal, Phys. Rev. B **78**, 155117 (2008).
[58] A. Kshetrimayum, H. Weimer, and R. Orús, Nat. Commun. **8**, 1291 (2017).
[59] Supplemantal Material.

Supplemental Material

In this Supplemental Material we briefly discuss additional simulation results that allow us to cross-check the findings of the main text.

In particular, from the simulations obtained using the infinite-size algorithm (iTEBD), we can check consistency of the exponents $\nu_\perp$ and β. This can be done by exploiting a scaling behavior of density-density correlations analogous to that of the time-dependent density curves.

Moreover, using instead a finite-size version of the algorithm we can check dynamical exponents of the non-equilibrium critical behavior of the QCP. On the one hand, we show how the estimate of the exponent δ, obtained by means of iTEBD, is compatible with that found from finite-system simulations. On the other hand, we will obtain estimates for an effective exponent z^{eff} (see last section of this Supplemental Material) using finite-size scaling derived from classical absorbing-state phase transition scaling theory. We will then compare this finite-size result with the z exponent estimated by means of infinite-size simulations (iTEBD). As we shall see, in order to match the two predictions, we need to enforce the effective dimension of the classical non-equilibrium field theory to be $d = 2$. Even considering the fact that our estimates are affected by error bars, this observation seems to indicate that a description of the quantum model by means of a non-equilibrium classical field theory should require an effective lattice dimension $d = 2$ for the latter.

Results from infinite-system simulations

In this first section of the Supplemental Material we present results from a scaling relation of the density-density correlations in the thermodynamic limit of infinite number of sites. This relation allows us to investigate the critical behavior of correlations at short distances; it therefore provides additional information about density-density correlations, which is complementary to that discussed in the main text. Indeed, the estimate presented in the main text is based on the asymptotic large-distance behavior of correlations which determines the divergence of the correlation length $\xi_\perp$, rather than on correlations between sites that are relatively close one to the other.

To be more precise, in this section we exploit the fact that density-density correlations in the steady-state ($C(r) = \langle n^{(r)} n^{(0)} \rangle - \langle n^{(0)} \rangle^2$) are expected to display an initial algebraic behavior $C(r) \approx r^{-\beta/\nu_\perp}$, for small enough r, and are then characterized by a universal function h, through the value of the correlation length $\xi_\perp \approx |\Omega - \Omega_c|^{-\nu_\perp}$. More concretely, one expects in the supercritical regime (below criticality stationary correlations are zero)

$$C(r) \approx r^{-\beta/\nu_\perp} h\left((\Omega - \Omega_c) r^{1/\nu_\perp}\right) , \tag{S1}$$

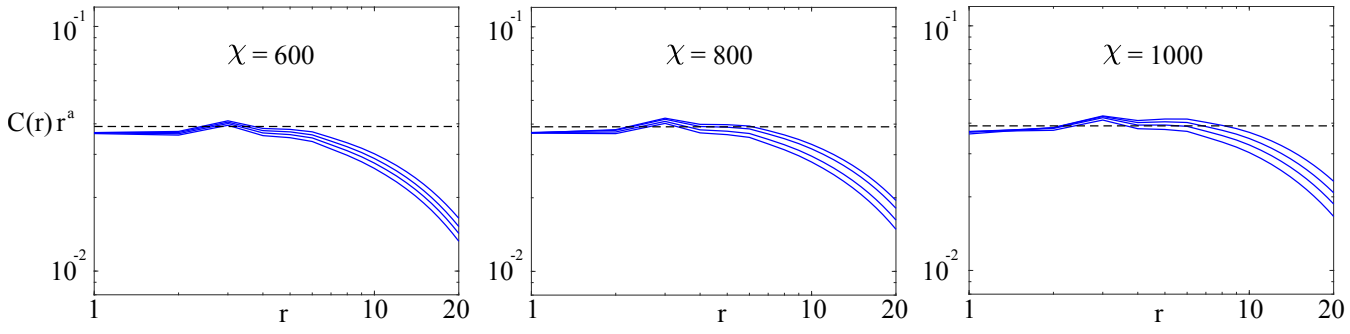

FIG. S6. **Infinite-system simulations.** The different panels display a log-log plot of the quantity $C(r)r^a$ as a function of r, for different values of the bond dimension χ. In each panel we show correlations for four different values of Ω (from $\Omega = 6.25$ to $\Omega = 7$, every 0.25) in the supercritical regime, as identified by the best estimate of the critical value $\Omega_c \approx 6$ discussed in the main text. For all bond dimensions considered, the value $a = 0.7$ collapses the different curves to an almost constant function for small enough values of r. As r increases the curves detach from the constant value and show exponential decay; this happens sooner for larger values of Ω –farther from Ω_c– since the correlation length becomes smaller and smaller in the supercritical regime. The value $a = 0.7$ is compatible with the value of $\beta/\nu_\perp$ obtained from the best estimate of the exponents discussed in the main text: $\beta/\nu_\perp \approx 0.36/0.5 = 0.72$.

with the universal scaling function h which is usually given by an exponential decay. Notice the similarity of the above equation with Eq. (3) in the main text, which, however, instead of spatial correlations involves time correlations.

Our goal is to estimate the ratio $a = \beta/\nu_\perp$ which appears in equation (S1). To this aim we consider the functions $C(r)r^a$ for different values of Ω, and we look for the value of a which collapses these curves onto a constant value for r small enough that the exponential decay governed by the correlation length has not yet kicked in. The larger the value of Ω, the sooner the exponential decay with r will become visible.

In Fig. S6 we show plots of $C(r)r^a$ as a function of r for different bond dimensions and at a sufficiently large time t. Focusing on short distances (small r), we see how the curves look almost constant when considering $a = 0.7$. This value of a is consistent with the ratio $\beta/\nu_\perp \approx 0.72$ obtained from the ratio of the best estimate of the two exponents. Importantly, the value of a seems to be much less sensitive to the bond dimension than what is observed for the correlation length $\xi_\perp$.

While this approach might not be suited for an a priori estimate of the exponent $\nu_\perp$, the trend that we have shown here, together with the estimated value of $\beta \approx 0.36$ (from the main text) constitutes, nonetheless, a good crosscheck for the reference value $\nu_\perp \approx 0.5$ estimated from the divergence of the correlation length.

Results from finite-system simulations

All quantitative results presented in the main text concern simulations which are performed by means of an iTEBD algorithm, which directly targets the thermodynamic limit of infinitely many sites enforcing the translation invariance of the system. This method allows one to eliminate one of the system parameters, namely the length of the chain L, as this is fixed to $L = \infty$. This algorithm is computationally much cheaper than a finite-system TEBD one, since the computational time of the latter has an extensivity with L which is not present in the iTEBD. Given that the bond dimension required by these dynamical simulations is quite large, this means that finite-size algorithms can only be adopted for relatively small sizes of the QCP. Nonetheless, even for the accessible intermediate sizes, a relatively good scaling behavior with L of the curves at criticality can be observed. This provides a partial check of the results obtained through infinite-system simulations.

Firstly, we exploit a relation predicted by classical field-theoretical arguments. The relation, valid at criticality, is

$$n(t) \approx t^{-\delta} \tilde{f}(t^{d/z}/L)\,; \tag{S2}$$

we can see how the dynamical exponent $z = \nu_\parallel/\nu_\perp$ appears conjugate to the dimension of the lattice of the classical field theory from which the scaling relation is derived. We thus, for the moment, define an exponent $z^{\text{eff}} = z/d$, and plot the critical density curves (at $\Omega = 6$) for different system sizes multiplied by t^δ as a function of $t/L^{z^{\text{eff}}}$. The scaling relation (S2) suggests that the so-constructed curves for different L should all collapse onto one master curve. In Fig. S7(a), we display this collapse, for sizes up to $L = 32$; the scaling behavior becomes evident for values of the exponents $\delta \approx 0.39$, in line with the one obtained with iTEBD, and for $z^{\text{eff}} \approx 1$. Such a value of the effective exponent z^{eff} is also confirmed by plots of the expected scaling of the gap (which we call μ) at criticality. From field theoretical arguments one expects, for the critical value of the branching rate, the relation $\mu \approx L^{-z^{\text{eff}}}$. In Fig. S7(b), it is displayed how this relation is satisfied by a value of $z^{\text{eff}} \approx 1$.

Such a result for z^{eff}, obtained from finite-size scalings, when compared with the value of z obtained from iTEBD seems to suggest that a valid non-equilibrium classical field theory describing the $1d$ QCP should display an effective classical dimension $d = 2$. Even if our iTEBD results are affected by error bars, it seems rather unlikely that these errors are so large that $z \approx 1$ should be expected.

Unfortunately, all scaling relations that can be obtained from field-theoretical arguments applied to our dynamical simulation scheme always involves the appearence of an effective $z^{\text{eff}} = z/d$ or of an effective $\nu_\perp^{\text{eff}} = d\nu_\perp$, so that a direct estimate of $\nu_\perp$ (and therefore of z through the relation $z = \nu_\parallel/\nu_\perp$) can only be done by looking at the divergence of the correlation length as we have done for our iTEBD results. In order to perform this latter analysis on finite-size systems we would need to reach substantially larger sizes. This is not feasible with current numerical methods. Notice indeed that, even for the relatively small sizes discussed in this Supplemental Material, we had to resort to the use of parallelization schemes on a cluster, while simulations from iTEBD have been produced on standard PCs.

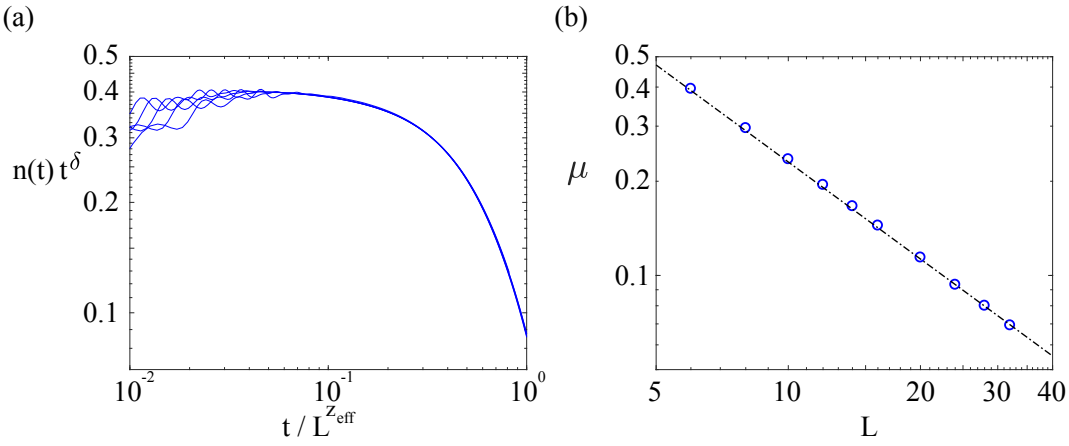

FIG. S7. **Finite-system simulations at the critical value of the branching field $\Omega = 6$.** (a) Plot of the scaled density curves $n(t)t^{\delta}$ as a function of $t/L^{z_{\rm eff}}$, for values of $L = 16, 20, 24, 28, 32$. Smaller values of L do not show a nice collapse as these sizes are not yet fully within the scaling regime, while larger values of L cannot be explored through the methods used here. The curves show a satisfactory collapse for $z^{\rm eff} = 1.03$ and $\delta = 0.39$. The latter value is in very good agreement with the one discussed in the main text. In fact we believe that the agreement could be even better but the value $\delta = 0.39$ seems to be slightly overstimated by the fact that we are still looking at relatively small system sizes. (b) Behavior of the gap of the Lindblad generator as a function of the size of the system ($L = 6, 8, 10, 12, 14, 16, 20, 24, 28, 32$). The gap has been estimated by fitting the late time exponential decay of the density curves for the different L. This procedure has been verified by comparing the results with those obtained from exact diagonalization for systems with size up to $L = 10$. The gap shows a power-law decay with the size of the system which agrees with the behavior $L^{-z_{\rm eff}}$ (shown by the dot-dashed line) with the $z_{\rm eff} = 1.03$ estimated from the collapse in panel (a). In both plots, all curves considered have converged in bond dimension (the maximal bond dimension employed is $\chi = 1300$), exception made for $L = 28$ and $L = 32$ which show some very small finite bond-dimension effect which, however, does not compromise the scaling behavior.